NANO LETTERS

Letter

pubs.acs.org/NanoLett

Near-Infrared Quantum Dot Emission Enhanced by Stabilized Self-Assembled J-Aggregate Antennas

Francesca S. Freyria,[†] José M. Cordero,[†] Justin R. Caram,[†,§] Sandra Doria,[†,‡] Amro Dodin,[†] Yue Chen,[†] Adam P. Willard,[†] and Moungi G. Bawendi*[,†]

[†]Department of Chemistry, Massachusetts Institute of Technology, Cambridge, Massachusetts 02139, United States

[‡]European Laboratory for Non Linear Spectroscopy (LENS), Università di Firenze, Sesto Fiorentino, Florence, 50019 Italy

Supporting Information

ABSTRACT: Enhancing photoluminescent emission (PL) in the near-infrared−infrared (NIR−IR) spectral region has broad applications from solar energy conversion to biological imaging. We show that self-assembled molecular dye J-aggregates (light-harvesting nanotubes, LHNs) can increase the PL emission of NIR PbS quantum dots (QDs) in both liquid and solid media more than 8-fold, promoted primarily by a long-range antenna effect and efficient Förster resonance energy transfer (FRET) from donor to acceptor. To create this composite material and preserve the optical properties of the nanocrystals, we performed an in situ ligand substitution followed by a functionalization reaction using click-chemistry. This resulted in PbS QDs soluble in an aqueous environment compatible with the molecular J-aggregates (LHNs). Theoretical and experimental results demonstrate that long-range diffusive exciton transport in LHNs enables efficient energy transfer to low concentrations of QDs despite there being no direct binding between molecular donors and QD acceptors. This suggests a broad application space for mixed light harvesting and photophysically active nanocomposite materials based on self-assembling molecular aggregates.

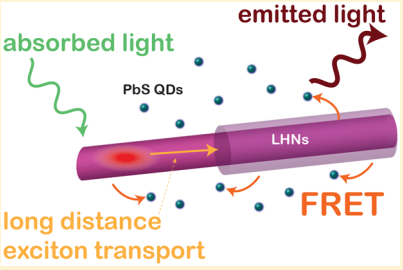

KEYWORDS: *NIR PbS QDs, water-soluble QDs, J-aggregates, antenna effect, FRET, excitons, hybrid materials*

Hybrid organic−inorganic nanocomposite materials create new synergies that open possibilities for light-harvesting applications.[1−6] For example, coupling conjugated organic dye molecules with semiconducting nanocrystals allows the narrow absorption and large oscillator strengths of organic dyes to combine with the wavelength tunability, high quantum yield, and stability of inorganic nanocrystals.[1,7,8] In such a system, organic nanostructures act as light-absorbing antennas, absorbing energy and delivering it to sparse inorganic nanocrystals, which then emit light or can be used for photochemical reactions. Such a system can deliver excellent performance under low-light and diffuse conditions, such as in sunlight or under LED illumination.

We report a simple design for an organic antenna/nanocrystal nanocomposite, which forms in water and can be stabilized in the solid state. Using self-assembled molecular dye aggregate (light-harvesting nanotubes or LHNs), we dramatically enhance the photoluminescence of infrared-emitting PbS quantum dots. The transport of energy from LHN to PbS NCs is mediated through rapid delocalization along the LHN structure followed by efficient Förster resonance energy transfer (FRET) in both liquid and solid media at room temperature. We demonstrate that LHNs act as efficient antennas, delivering energy over long distances to QDs within a dilute nanocrystal solution. Using a theoretical model, we illustrate that energy mobility is significantly enhanced by the self-organization of dye molecules into LHNs and that this enhancement is primarily responsible for the observed antenna effects. These results thus suggest a simple indirect strategy for enhancing the effective oscillator strength of QD materials, which can be extended to a wide range of different composite materials.

Our antenna system is a molecular J−aggregate that self-assembles from amphiphilic cyanine dyes into extended tubular structures with narrow absorption features, and which has been shown to display long-range excitation energy migration due to strong interaction between the transition dipole moments of the dye monomers.[9−11] LHNs consist of C8S3 monomer molecules (3,3′-bis(2-sulfopropyl)-5,5′,6,6′-tetrachloro-1,1′-dioctylbenzimidacarbo cyanine) that aggregate in water into quasi-one dimension cylindrical structures, forming two well-defined concentric nanotubes, with the outer tube 12 nm in diameter, the inner tube 6 nm in diameter, and with lengths of several microns.[10,12,13] Over longer time scales, these double-walled nanotubes further self-assemble into bundled tubular structures.[14,15] These close-packed structures still preserve the efficient excitation energy transport properties of the building units and also act as considerably strong light-harvesting antennas.[15,16]

In this experiment, we chose PbS quantum dots as acceptors for their wide tunable emission energies from 0.6 to 1.8 eV, which covers the silicon solar cell band gap for luminescent

Received: August 30, 2017
Revised: November 1, 2017
Published: November 17, 2017

DOI: 10.1021/acs.nanolett.7b03735
Nano Lett. 2017, 17, 7665−7674

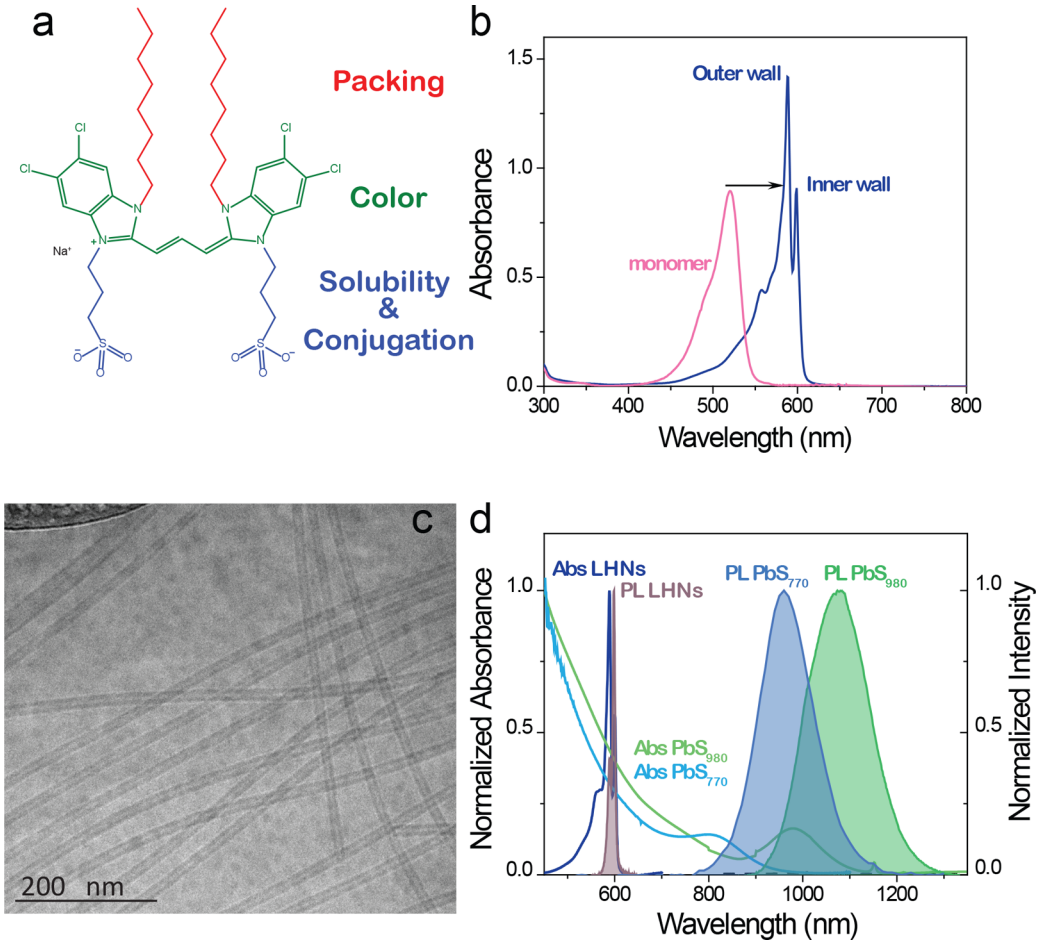

Figure 1. (a) C8S3 monomer molecular structure. (b) Absorption spectra of LHN system: absorption spectrum of C8S3 in methanol (pink line) and absorption spectrum of self-assembled LHNs after adding monomer methanol solution to water (0.26:1 v/v ratio). The absorption spectrum indicates a double-walled nanotube morphology (blue line). (c) cryo-TEM image of double-walled LHNs. (d) Normalized optical spectra of the two hybrid systems in aqueous solution: absorption and PL spectra of LHNs as donor and absorption and PL spectra of PbS_{770} and PbS_{980} as acceptor (light blue lines and green lines, respectively).

solar concentrator and photovoltaics applications.[17,18] Moreover, PbS QDs can be applied in other several fields, such as short-wavelength infrared (SWIR) optical communications[19,20] and deep tissue bioimaging.[21] Synthesized PbS QDs are generally incompatible with water due to the native aliphatic ligands employed during synthesis.[22−26] To render QDs water-soluble, they are typically modified with a suitable hydrophilic coating after synthesis using a ligand exchange,[27−34] encapsulation,[35] or a silica-coating process.[36] However, these procedures generally decrease their optical stability and can increase the particle size distributions.[6,33,37−40] Here, we describe a new method for preparing aqueous QDs that utilizes a modified aliphatic ligand possessing a norbornene motif, which is added directly during synthesis, and can be used to disperse the QDs in water after clicking to a polyethylene glycol head group (PEGylation). This technique maintains the native synthesis ligands in place and preserves the final quantum yield and particle size distribution of the QDs in water over several months (Figure 2).

Energy transfer (ET) from organic dye molecules to QDs is not typically efficient due to the relatively weak dipole in nanocrystals. As a result, organic dyes can act as acceptors in the presence of QDs donors but are typically mediocre donors, mostly attributable to the dominance of a fast radiative decay channels of the donor dye relative to the slower nonradiative FRET decay channel into the QD acceptor, especially when dyes are covalently attached to engineered binding proteins coordinated on QD surfaces.[41] Our observations demonstrate that molecular aggregates with high exciton diffusion lengths and strong transition dipoles can enhance the energy transfer between organic dyes and sparse QDs, suggesting general design principles for dye enhanced QD materials.[42]

In 1999, Basko et al. predicted efficient Förster resonant energy transfer from 2D semiconductor quantum wells[43] or quantum dots[44] to an organic bulk material. Since then, energy transfer from inorganic nanocrystal (with primarily Wannier−Mott delocalized excitons) to organic compounds (with localized Frenkel Excitons) and the reverse have been reported extensively.[5,7,41,45] For example, highly efficient energy transfer between J-aggregates and inorganic semiconductors has been accomplished in a number of systems including: core/shell CdSe/ZnS QDs coupled either with J-aggregates of the cyanine dye TDBC through PDDA as molecular glue in hybrid films[1] or with TTBC J-aggregates electrostatically coupled through a charged amphiphilic polymer in solution;[7] core/shell CdSe/ZnCdS QDs coupled with thiacyanine J-aggregate (TCJ) and carbocyanine dye (BIC) J-aggregate through 2-mercaptoethyl-*N*,*N*,*N*-trimethylammonium chloride (mta) and 3-merpcapto-1-

DOI: 10.1021/acs.nanolett.7b03735
Nano Lett. 2017, 17, 7665−7674

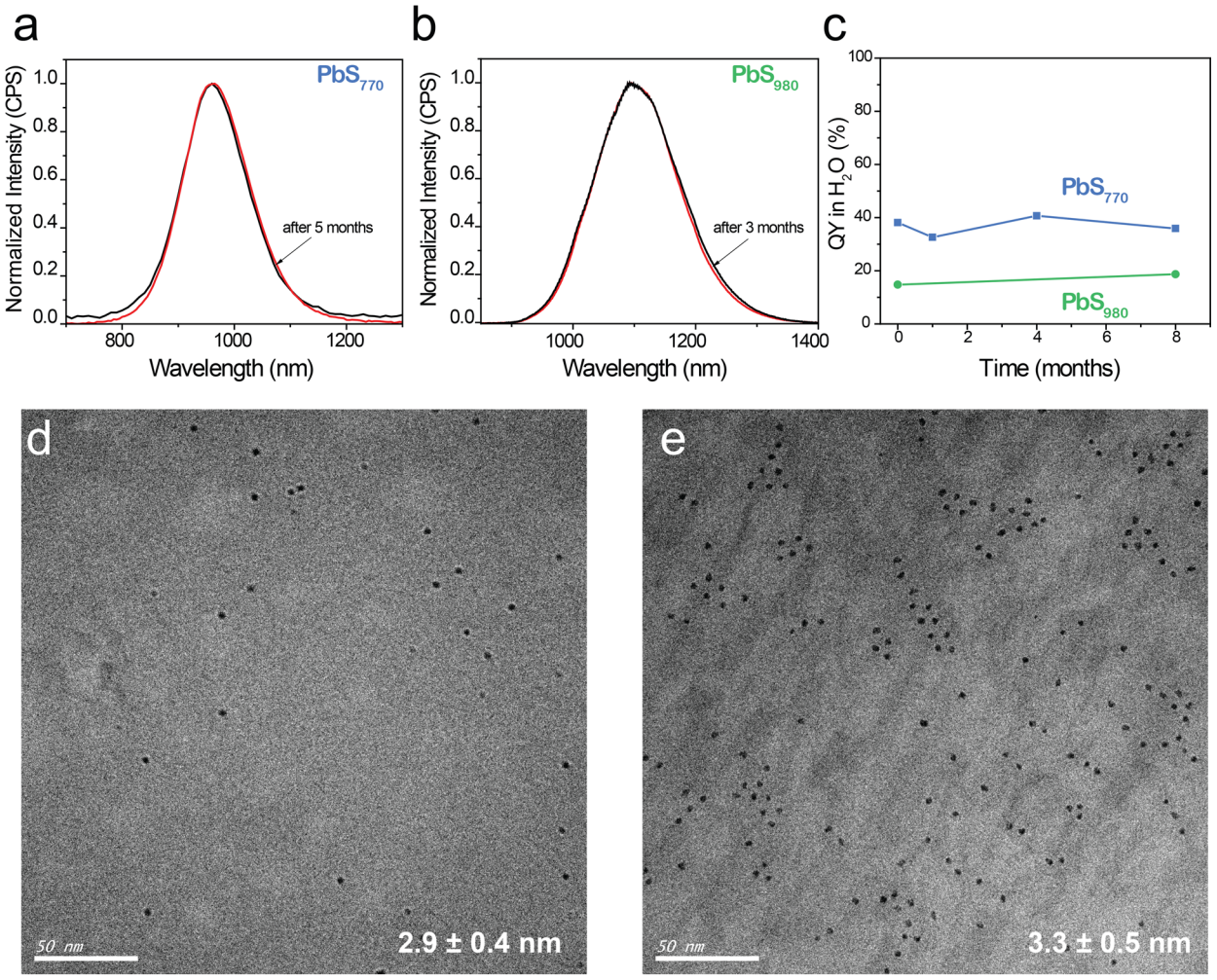

Figure 2. Stability of water-soluble QDs over months: (a) PL emission spectra of PbS_{770} (black line), red line after 5 months; (b) PL emission spectra of PbS_{980} (black line), red line after 3 months; (c) QY in water of PbS_{770} (blue line) and PbS_{980} (green line); (d) cryo-TEM image of PbS_{770} in water; and (e) cryo-TEM image of PbS_{980} in water.

propanesulfonate (mps) ligands;[8] and J-aggregates from amphiphilic cyanine dye C8S3 covered with poly-(diallyldimethylammonium chloride) (PDADMAC) coupled to MPA-capped CdTe QDs.[46] In the infrared region, Wang et al.[34] have shown FRET from lead sulfide quantum dots to IR140-Cy^+ J-aggregates and, during the finalization of this publication, they have reported a two-step FRET relay in a composite film between donor and acceptor PbS/CdS through IR140-Cy^- J-aggregates as exciton bridge.[47] A commonality among all of these composites is direct coupling between inorganic nanocrystal and dye, either through electrostatic coupling or through dye-labeled ligand conjugation.

In this work, we show that LHNs can act as excellent light-harvesting antennas, greatly enhancing the emission of infrared quantum dots without directly conjugating the QDs to an organic J-aggregate system. Furthermore, self-assembly in water enables straightforward methods for solid-state encapsulation, which is critical for applications. This opens opportunities to create host−guest systems with large Stokes shift in the visible and all the way into the NIR-IR, effectively separating the absorption and the emission of the nanocomposite and displaying an extremely high tunable oscillator strength at a specific narrow wavelength range. Furthermore, an efficient antenna effect allows for low loading densities of heavy-metal-containing compounds, common in QD-based devices, and also limits their dispersion in environmentally hazardous organic media, such as hexane, toluene, and chlorinated solvents. Our observation of surprisingly high energy-transfer efficiencies in this mixed system can have application in many fields, spanning from solar devices,[1,48,49] light-emitting diodes,[50] optoelectronics applications,[5] biosensing,[6] sensitizing photocatalytic devices,[51] and photon down-conversion.[8]

Energy Transfer from LHNs to PbS Quantum Dots. C8S3 monomer is an amphiphilic cyanine dye whose structure can be divided in three main parts (Figure 1a): (i) a hydrophilic domain composed of a sulfonate terminated alkyl chain; (ii) a hydrophobic alkyl chain, which promotes a molecular bilayer configuration in water; (iii) a polymethine chain, whose length determines the spectral absorption features. If water is added to a solution of dye in methanol, the amphiphilic nature of the dye due to polarity change induces self-assembly into a helical three-dimensional structure, in which the monomers are packed together in a double folded sheet that form the two cylinders of the LHNs (Figure 1c). The two absorption peaks centered at 590 and 600 nm arise from the outer and inner wall parallel transitions, respectively (Figure 1b). The cylindrical surface is formed by molecules structured in an organized brick-like geometrical pattern[9,13] with their transition dipoles coupled in a

DOI: 10.1021/acs.nanolett.7b03735
Nano Lett. 2017, 17, 7665−7674

Scheme 1. Reaction Sketch of PbS Coated with a Mix of Oleic Acid (Dark Grey) and Norbornene Acid (Green) with a Tz−PEG molecule (Fuchsia and Blue, Respectively)

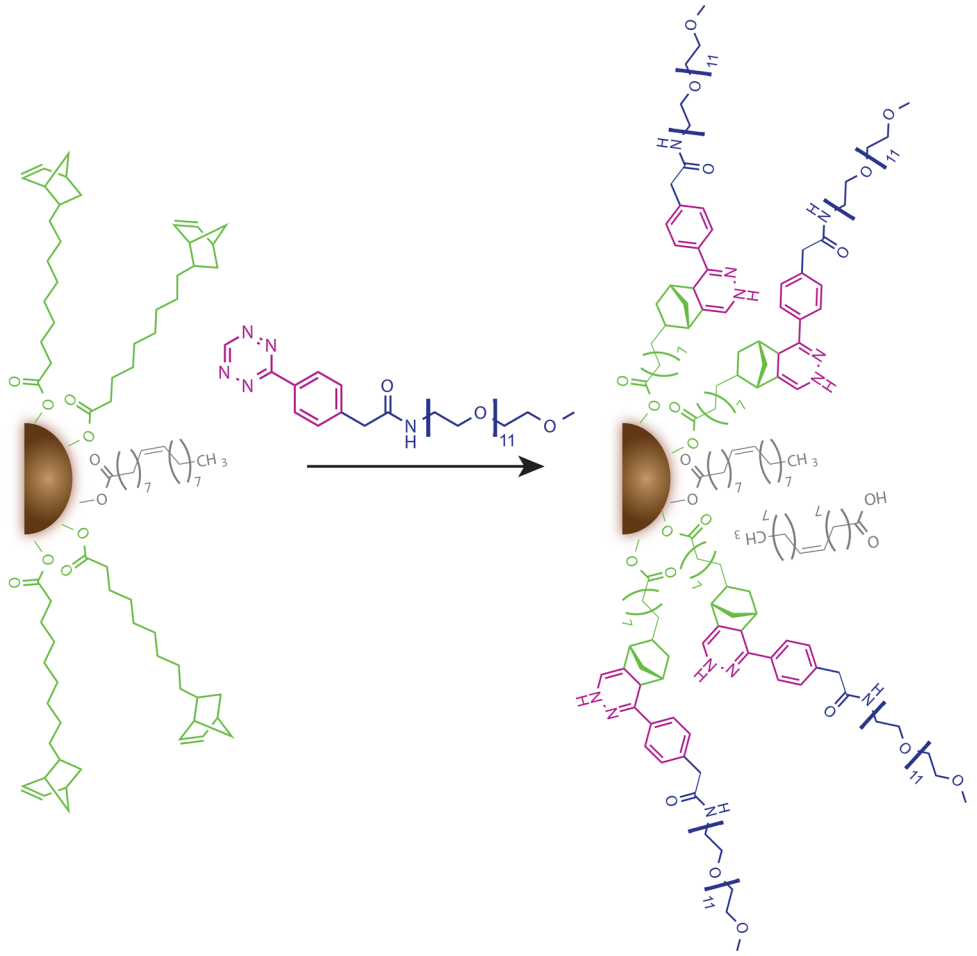

primarily "head to tail" arrangement, leading to a net negative coupling energy, as is expected for J-aggregation. The lowest-energy state is highly emissive, giving rise to an absorption band red-shifted relative to the monomer by 70 nm, with a large delocalized transition dipole, which leads to narrow spectral features with high oscillator strengths and fast radiative rates (Figure 1b), according to a J-aggregate structure. The J-type geometry facilitates a distributed transition dipole with coherent delocalization across multiple molecules, creating a cooperative emission, an increase of the radiative rate and as a result an increase in the quantum yield. This phenomenon is called superradiance.[52] We studied the energy-transfer process in both aqueous solution and sugar glass derived from a highly concentrated solution of sucrose and trehalose.[42] A pair of differently sized acceptor PbS QD ensembles, denoted by their respective absorption maxima, 770 nm (PbS_{770}) and 980 nm (PbS_{980}), were used (Table S1), and we show antenna enhancement of their emission both in solution and in solid matrix. The normalized absorption and emission spectra of these acceptor species are shown in Figure 1d. The band emission of the J-aggregates overlaps with the continuum of electronic states for PbS QDs, ensuring FRET energy transfer.

Preparation of Water-Soluble PbS Quantum Dots. Ligand exchange is a common route for obtaining water-soluble QDs. This method often causes a large decrease in quantum yield, a significant peak emission shift, and may also perturb the particle size distribution, leading to broader emission line widths, limiting the application space for water-soluble QDs.[6,26,53] This is more evident for the near-infrared and infrared emitting nanocrystals, whose optical quality even in organic phases is still not as high as for the visible-light-emitting QDs. Furthermore, the lack of reliable methods to produce type I core−shell structures in PbS, which confine the exciton to the core and away from surface-related electronic trap states, makes this system particularly sensitive to ligand exchange.

We applied a new method for the synthesis of PbS QDs coated with norbornene functional groups for facile derivatization, by synthesizing a new norbornene mono acid ligand (details in S.I.). Our approach takes advantage of previously reported methods that use oleic acid as the only passivating surface ligand.[23] A carboxylate-based ligand possessing a terminal norbornene residue is added to the reaction mixture in partial substitution of oleic acid. The resulting norbornene-coated PbS QDs display a QY in chloroform equal to 65% and 55% for PbS_{770} and PbS_{980}, respectively. The QDs are PEGylated using tetrazine-functionalized PEG (PEG-Tz), which reacts with the norbornene ligand through an inverse electron-demand Diels−Alder cycloaddition. The final QY in water drops to 38% for the smaller QDs (PbS_{770}) and to 18% for the bigger QDs (PbS_{980}) used in this study (Table S1). Both QD batches show a high optical stability for more than 8 months (Figure 2), with a QY standard deviation in water around 3% (Figure 2c). The morphology of the PEG−Tz−QD constructs is still preserved in the aqueous system, with no

DOI: 10.1021/acs.nanolett.7b03735
Nano Lett. 2017, 17, 7665−7674

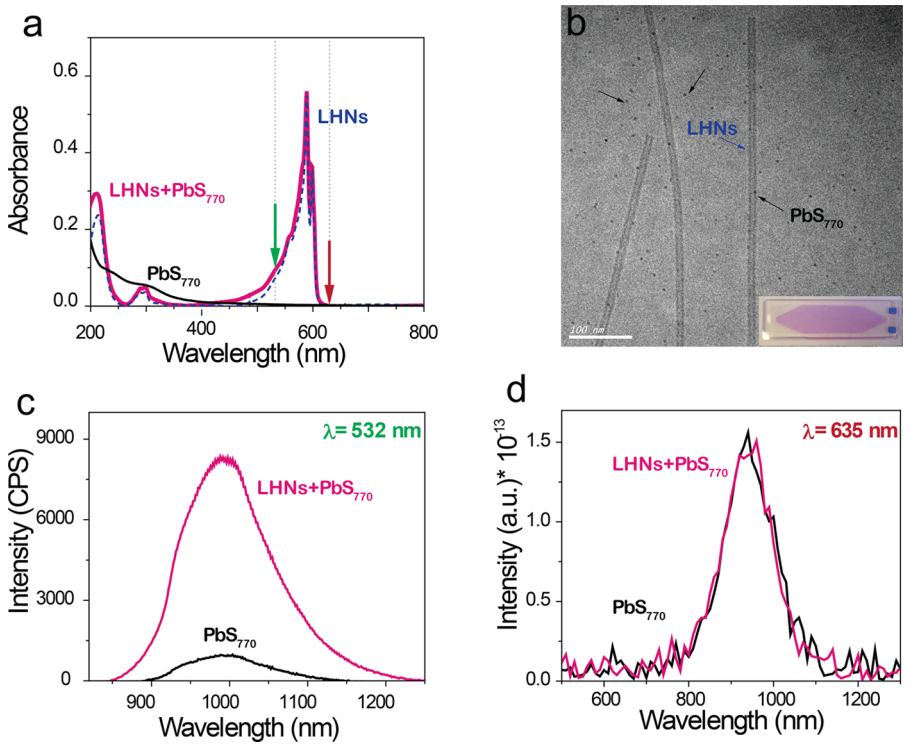

Figure 3. Optical spectra of LHNs coupled with PbS_{770} QDs in aqueous solution. Purple line: LHNs coupled with PbS_{770} QDs. Blue dashed line: LHNs control sample. Black line: PbS_{770} QDs control sample. (a) UV−vis absorption of the three samples; green and red arrows indicate the excitation at 532 and 635 nm, respectively. (b) Cryo-TEM image of the LHNs coupled with PbS_{770} QDs in aqueous solution; inset sample in a 0.1 mm cuvette. (c) PL spectra of LHNs coupled with PbS_{770} and PbS_{770} control samples excited at 532 nm (green arrow in panel a). (d) PL spectra of LHNs coupled with PbS_{770} and PbS_{770} control samples, excited at 635 nm (red arrow in panel a).

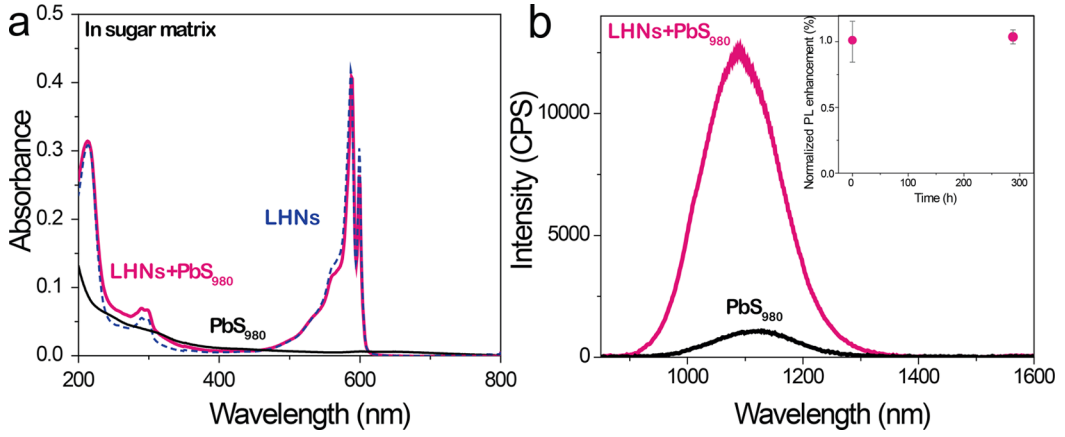

Figure 4. Optical properties of LHNs coupled with PbS_{980} QDs in sugar matrix, LHNs coupled with PbS_{980} QDs (purple line), LHNs control sample (blue line), and PbS_{980} QDs control sample (black line). (a) UV−vis absorption of the three samples. (b) PL spectra of LHNs coupled with PbS_{980} and PbS_{980} control sample excited at 532 nm; inset: normalized PL enhancement of QDs over time. The samples were kept under room light, and the PL enhancement was measured after 12 days.

agglomeration observed either in cryo-TEM images (Figure 2d,e) or in the particle-size distribution (Figure S2a). These particles retain a net negative surface charge in water (Figure S2b), probably due to the presence of intercalated free carboxylic acid ligands into the organic shell (Scheme1).

Double-Walled LHNs Coupled to QDs in a Liquid System. The absorption spectrum of the LHN+QD system is reported in Figure 3a, where the two features typical of double-walled nanotubes are preserved in the nanocomposite spectrum (LHNs + PbS_{770}). Cryo-TEM (Figure 3b) shows that only ∼10% of the QDs are within a typical FRET radius R_0 (∼7.5 nm, vide infra, eq 2). Assuming the most-sensitive distance range for FRET is 0.5 R_0−2R_0,[54] less than 15% of the dots are in the right range to efficiently contribute to energy transfer (Figure S3). To quantify the contribution of the J-aggregates to the QD emission, we compare the emission spectra of the QDs in the presence and in the absence of LHNs (Figure 3c,d). We excited the system at two different wavelengths, 532 and 635 nm (green and red arrows, respectively, in Figure 3a), within and at a longer wavelength than the absorption band of the LHNs, respectively. In the LHNs absorption range, we chose as excitation wavelength 532 nm to ensure absorption in the low-

DOI: 10.1021/acs.nanolett.7b03735
Nano Lett. 2017, 17, 7665−7674

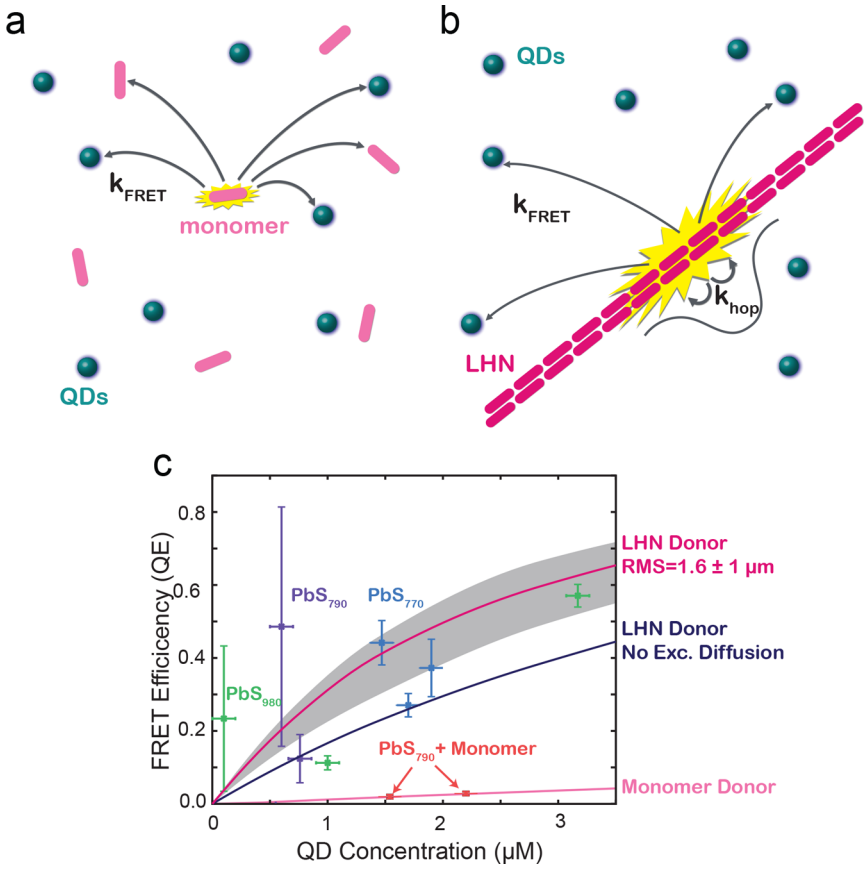

Figure 5. (a) Schematic of dye monomers (pink) with QDs (blue). Excitons are initialized on randomly chosen monomers, and FRET rates to each donor and each acceptor are calculated. They are then allowed to hop between donors until a transfer event to an acceptor or an exciton decay event occur. If the acceptor transfer event occurs first, it contributes to the FRET efficiency. (b) Schematic of a section of LHN (purple) with QDs (blue). Excitons are placed on LHN and allowed to freely diffuse with a given root-mean-square displacement (RMS). FRET rates are calculated at each position, and if an acceptor event occurs before an exciton decay event, it contributes to the FRET efficiency. (c) We plot the FRET quantum efficiency of eight different concentrations of QDs with three different emission wavelengths. We compare this to the quantum efficiency of transfer for two samples of monomer and QD systems in methanol. The solid lines represent simulations for the monomer + QD system, the LHN + QD system, and LHN + diffusion + QD system. The gray-shaded region shows the range of theoretical predictions obtained for RMS diffusion lengths between 0.6 and 2.6 μm. The predicted QE enhancement increases monotonically with increasing RMS diffusion lengths. We observe enhancement due to increased QY of the aggregate and contributions from long-range exciton diffusion along the aggregate.

wavelength region of the spectrum and to avoid electronic-state saturation. The PL emission of the QDs increases up to eight times on average when only the J-aggregates are excited at 532 nm, (green arrow, Figure 3c), whereas the emission intensity of QDs remains unchanged when the sample is excited outside the LHN's absorption band at 635 nm (red arrow, Figure 3d). We observed the same behavior in the system formed by LHNs coupled with lower-energy-emitting quantum dots, PbS_{980} (Figure S4). Furthermore, the excitation spectrum of the coupled system collected by monitoring the QD emission above 850 nm shows features similar to the outer- and inner-wall absorption transition of LHNs in the range 550−610 nm, suggesting that the exciton from LHNs absorption in the visible range enhances the nanocrystal emission in the infrared region (Figure S5).

LHNs Coupled to QDs in a Solid System. We also investigated the excitation energy transfer in a photostable solid matrix. The samples were prepared by following the "sugar route" by starting from LHNs in aqueous solution.[42] The morphology as well as all the typical absorption features of LHNs are maintained in the stabilized matrix samples, either in the presence or in the absence of QDs, as in the liquid sample (Figures 4 and S7). The double-walled nanotubes morphology is still preserved, and the distribution of the QDs around them does not show any significant differences compared to the solution. The integrated area under the emission curve of QDs in the presence of LHNs shows an enhancement comparable to the solutions for both systems (PbS_{770} and PbS_{980}; Figures 4 and S7). The samples were stored under room light in vacuum condition to avoid any degradation of the sugar glass matrix. Under these conditions, the PL enhancement of QD emission shows a constant behavior after 12 days (Figure 4b).

Modeling the Effect of Supramolecular Self-Assembly on Energy-Transfer Efficiency. When isolated dye molecules self-assemble, their optoelectronic properties can change significantly. For instance, this is highlighted in the spectral shift in Figure 1b. These changes reflect an increase in intermolecular electronic coupling between self-assembled dye molecules, which allows electronic excitations to be shared among many individual dye molecules. The mobility, spatial characteristics, and emissive properties of these delocalized excitations can differ significantly from that of the isolated molecules. To explore how these differences influence the efficiency of dye-to-QD energy transfer, we have constructed a simple coarse-grained model of this system. Our model reveals that the quantitative enhancement of QD emission observed

DOI: 10.1021/acs.nanolett.7b03735
Nano Lett. 2017, 17, 7665−7674

experimentally can be attributed partially to an increased mobility of excitons within the supramolecular LHN.

Our model includes a fixed number of QDs distributed randomly within a periodically replicated cubic simulation cell of 27 cubic microns. The cell also includes a fixed number of dye molecules that are either distributed randomly in space to simulate the nonaggregated monomer mixture or arranged in a linear array to simulate the self-assembled supramolecular LHN. The simulation includes N_D donor (dye) molecules, N_A acceptor (QD) molecules, and a single exciton. The positions of the donor and acceptor molecules are fixed; however, the exciton can move within the system. The exciton dynamics are governed by a simple Markov chain model that is propagated with a kinetic Monte Carlo algorithm. In this model, we assume that excitons are localized on individual molecules in the nonaggregated monomer system and delocalized across many individual molecules in the aggregated LHN system. We therefore model exciton dynamics differently in these two systems (Figure 5a,b).

For the nonaggregated monomer system exciton transport is mediated by intermolecular energy transfer, which we model based on the theoretical formalism of FRET. Specifically, the rate of transfer from one molecule to another is given by:

$$k_{FRET}(R) = \left(\frac{R_0}{R}\right)^6 \tau_D^{-1} \tag{1}$$

where R is the distance between the two molecules, τ_D is the radiative lifetime of the donor, and R_0 is the so-called Förster radius as given by:

$$R_0 = \left(\frac{9(\ln 10)\kappa^2 \Phi_D}{128\pi^5 N_{AV} n^4} J\right)^{1/6} \tag{2}$$

where N_{AV} is Avogadro's number, κ is an orientation factor, Φ_D is the donor fluorescence quantum yield and n is the refractive index of the medium (taken to be 1.33 for methanol and water). Here, J is a function:

$$J = \int f_D(\lambda)\epsilon_A(\lambda)\lambda^4 \, d\lambda \tag{3}$$

that describes the overlap between the normalized donor emission, $f_D(\lambda)$, and acceptor extinction coefficient, $\epsilon_A(\lambda)$, expressed in terms of wavelength, λ. We assume that dye molecules reorient rapidly relative to the excited-state lifetime and thus set the orientation factor κ^2 equal to 2/3. Excitons are initialized on a random donor molecule and then propagated with a rejection-free kinetic Monte Carlo algorithm (rfkMC) that includes all possible molecule-to-molecule transitions (both donor−donor and donor−acceptor) and the possibility for radiative recombination with a rate $k = 1/\tau_D$. A trajectory is terminated if the exciton undergoes donor recombination or if the exciton transfers to an acceptor molecule (here, we assume that the acceptor radiates immediately upon excitation). We generate many trajectories with many different molecular configurations and compute the energy-transfer efficiency by computing the fraction of trajectories that terminate via acceptor occupation.

For the aggregated LHN system, we assume that excitons delocalize along the array and, thus, have a centroid position that varies continuously along the axis of the dye aggregate. We model the dynamics of the exciton position within the aggregate as a one-dimensional Gaussian random walk. In addition, from any position along the aggregate the exciton can undergo FRET transfer to any of the N_A QD acceptors with the FRET rate of eq 1 or recombine on the donor aggregate with a rate $k = 1/\tau_D$. This model is propagated using a two-step rfkMC process. First, a KMC process is used to determine if the exciton undergoes donor recombination, undergoes FRET to a quantum dot, or remains on the aggregate. Then, if the exciton remains on the aggregate, it takes a step in a 1D random walk along the linear aggregate drawn from a Gaussian distribution. This two-step process is repeated until the exciton either recombines or transfers to a donor molecule. Similar to the case of the nonaggregate monomer system, we compute energy-transfer efficiency by averaging over many individual trajectories with many different molecular configurations. This approach is consistent with a fully quantum multichromophore FRET treatment in the incoherent limit where the decoherence time in the site basis is far shorter than the other system time scales. In this case, the trajectory averaged exciton distribution is equivalent to the diagonal elements of the site-basis density matrix, and all off-diagonal elements vanish. Recent reports have shown that LHNs can transport energy from 180 to 1600 nm along their longitudinal dimension.[42,55] To account for this variability in diffusion length, we simulate the exciton dynamics for a range of RMS diffusion lengths from 0 to 3600 nm and present the theoretical predictions as the gray shaded region in Figure 5c.

The physical constants that determine the Förster radius (eq 2) and, thus, the FRET rate are denoted in Table 1. Notably, these constants differ significantly between the monomer and aggregate systems. This difference reflects changes in the excitonic properties between the localized and delocalized excitons. Furthermore, the overlap integrals differ for donor-to-donor and donor-to-acceptor transfer in the monomer case giving the following FRET radii. $R_{D\to D}^{(Monomer)} = 5.1$ nm, $R_{D\to A}^{(Monomer)} = 6.6$ nm, and $R_{D\to A}^{(Aggregate)} = 7.5$ nm. Note that donor-to-donor transfer is neglected in the aggregate case as typical aggregate to aggregate spacing far exceeds the FRET radius. In both monomer and LHN simulations, we consider a variety of donor concentrations from 0.2 to 3.2 μM (five points) and use a cubic spline interpolation for a smooth line.

Table 1. Experimental Parameters Corresponding to Monomer and Aggregate Model Simulation[a]

	donor concentration [mM]	acceptor concentration [μM]	τ_D (ps)	Φ_D (%)	l_D (μm)
C8S3 (monomer)	0.4	[0.2−3.2]	240	1.5	–
LHN (aggregate)	0.4	[0.2−3.2]	90	15	0−3.6

[a]The parameter l_D gives the diffusion length of the exciton on the linear aggregate.

In Figure 5c, we compare the results of the simulation to the measured quantum efficiencies of energy transfer from both LHNS and monomer units as donors to PbS quantum dots as acceptors. To quantify the quantum efficiency (QE) of energy transfer, we use the following equation:

$$Em_{D+A} = Abs_A \cdot \Phi_A + Abs_D \cdot \Phi_A \cdot QE \tag{4}$$

$$QE = \left(\frac{Em_{D+A} - Em_A}{Em_A}\right) \Big/ \frac{Abs_{D+A} - Abs_A}{Abs_A} \tag{5}$$

DOI: 10.1021/acs.nanolett.7b03735
Nano Lett. 2017, 17, 7665−7674

where Em_{D+A}, Em_A, Abs_{D+A}, and Abs_A are the emissions and the absorption of the acceptor in the presence and in the absence of the donor, respectively, at the same excitation wavelength, and Φ_A, defined as Em_A/Abs_A, is the quantum yield of the acceptor, which we assume stays unchanged in the presence of the donor. We define the QE as the probability that an exciton from the donor reaches the acceptor. Eq 5 is then the ratio between the observed enhancement and the maximum potential enhancement. We calculate the error bars in Figure 5c using standard propagation by assuming an error bar of 0.002 OD in absorption. Generally, as the QD concentration increases, the quantum efficiency of FRET increases. We observe between 0.3 and 0.6 transfer efficiency for LHNS to quantum dots compared with 0.03 and 0.05 transfer efficiency for monomer donors to quantum dot acceptors. For comparison to simulation (solid lines), we rescale the maximum transfer rate by 0.3 to match the experimental monomer−QD QE. Our results show that two effects greatly enhance the efficacy of LHN sensitization. First, the increase overall quantum yield of the aggregates (due to delocalized transition dipoles resulting in faster radiative rates) increases the overall FRET rate. The second enhancement is a nonlinear increase in the QE due to exciton diffusion. As is shown in Figure 5c, aggregate enhanced QY cannot account for the large QE observed in several samples. Due to the strong distance dependence of FRET rates, a given exciton has a fairly low probability of leaving the donor subsystem unless it enters a high FRET rate region. This leads to a disproportionate enhancement of donor to acceptor transfer in systems with more mobile excitons, accounting for the observed "antenna" effect.

Conclusions. We have reported a new, efficient method by which to synthesize water-soluble infrared quantum dots, which highly preserve the optical properties of the nanocrystals and allow an easy functionalization via the click-chemistry process. Using these nanocrystals, we demonstrate significant PL enhancement of NIR-emitting QDs in the presence of LHNs in both liquid and highly stable solid matrices. Despite weak physical and energetic coupling between subsystems, we observed that LHNs act as light-harvesting antenna through efficient funneling to regions of strong FRET where significant donor−acceptor transport occurs. The relative simplicity of this system, its water compatibility, and the large enhancement of the emission from highly dilute QDs suggest applications to a broad range of photochemical and photoelectric systems.

Water-Soluble PbS QDs Preparation. PbS QDs were synthesized based on Hines et al. synthesis.[23] Briefly 0.306 g of lead acetate trihydrate (Sigma-Aldrich, 99.99 purity) were dissolved in 8 mL of 1-octadecene (ODE, Sigma-Aldrich, technical grade) with oleic acid (OA, Sigma-Aldrich, technical grade) to have a fine concentration ∼0.1 M. Next, the solution was degassed at 80 °C for at least 2 h. In the glovebox, 105.5 μL of hexamethyldisilathiane (Sigma-Aldrich, synthesis grade) was dissolved in 5 mL of ODE and then quickly injected in the flask with the lead precursor. In our synthesis OA was partially (25%−75% mol) substituted by norbornene acid (NA, synthesis procedure in the Supporting Information) directly during the synthesis. The two batches were obtained by changing the quenching temperature (60 and 85 °C, respectively). QDs were centrifuged with acetone to separate the QDs from the growth solution. The supernatant was discarded, and the QDs were rewashed with hexane and acetone. Finally, the functionalized QDs were dispersed in chloroform and stored in inert atmosphere. Before dispersing in water, the nanocrystals were mixed with Tz−PEG (the synthesis procedure is given in the Supporting Information) and left stirring overnight (Scheme 1) under inert atmosphere. Next, water-soluble nanocrystals were purified by filtration tubes (Amicon Ultra, 10 kDa) three times with methanol and deoxygenated double-distilled water. The QDs in double-distilled water were stored in a glovebag under N_2. This new synthesis method eliminates the need for ligand exchange and confers a very high quantum yield and a high optical stability over months in water (Figure 2).

Ligand Preparation. The ligand was prepared according the method explained in the Supporting Information.

Preparation of Double-Walled J-Aggregates. J-aggregate nanotubes were prepared via a slightly modified "alcoholic" (water/methanol) route. Stock solution of C8S3 (3,3′-bis(2-sulphopropyl)-5,5′,6,6′-tetrachloro-1,1′-dioctylbenzimidacarbocyanine) was prepared by directly dissolving the sodium salt powder (FEW Chemicals, Germany) in methanol to reach a final concentration of 2.92 mM. Then, 260 μL of the C8S3 monomer solution was added to 1000 μL of double deionized H_2O, softly mixing and stored in the dark for 24 h. Fresh J-aggregate solutions were stored in the dark and used within 1 day after preparation.

Surface-Charge and Particle-Size Distribution. Particle surface charge was measured by gel electrophoresis. The gel was prepared by dissolving 0.5 g of LE Agarose (GeneMate) in 50 mL of Tris−acetate buffer at 80 °C. The images were taken by custom imaging setup with a 10 W 808 nm laser (Opto Engine; MLL-N-808) coupled in a 910 μm core metal-clad multimode fiber (Thorlabs; MHP910L02) and InGaAs camera (Princeton Instrument, NIRvana). The laser light was blocked with both an 850 nm long pass filter and an 850 nm long pass dielectric filter (Thorlabs, FELH0850).

Gel filtration chromatography (GFC) was performed using an ÄKTA Prime Plus chromatography system from GE Healthcare Life Sciences equipped with a Superose 6 10/300 GL column. PBS (pH 7.4) was used as the mobile phase with a flow rate of 0.5 mL/min. Detection was achieved by measuring the absorption at 280 nm.

Preparation of PbS/LHNs Assembly. The liquid samples were prepared by mixing 20 μL of water-soluble PbS dispersion at different concentrations with 200 μL of J-aggregates. The final dispersion was stored in dark for another 3−5 h to equilibrate. A pair of control samples were also prepared: (i) 20 μL of double distilled water was added to 200 μL of J-aggregates solution, and (ii) 20 μL of water-soluble PbS dispersion was diluted with 200 μL of double-distilled water. All the optical characterizations were taken in 0.1 mm path length quartz cuvettes (Starna).

The sugar matrix samples were prepared by following the "sugar route" method explained in Caram et al.[42] Briefly, 1:1 v/v of Jaggregates/PbS solution was mixed with sugar solution (50 wt % sucrose and 50 wt % Trethalose, Sigma-Aldrich) and left in a vacuum system for at least 48 h. The control samples were prepared by using the solutions of the control liquid samples and following the same procedure. All of the optical characterizations were taken in 0.2 mm path length quartz cuvettes (Starna). The stability test was conducted by keeping the samples for 12 days in a desiccator under room light. Due to a possible thickness inhomogeneity, three different points were measured for each sample.

Morphological Characterization. The morphology of the samples were investigated by cryo-TEM. Cryo-samples were

DOI: 10.1021/acs.nanolett.7b03735
Nano Lett. 2017, 17, 7665−7674

prepared by dropping ~10 μL of liquid sample solutions on lacey grids coated with a continuous carbon film (Lacey Formvar stabilized with Carbon, 200 mesh). Before use, the copper grids were hydrophilized by an oxygen plasma treatment for 10 s, performed with a Salaries Advanced Plasma cleaning system, Gatan Inc. To remove sample in excess without damaging the carbon layer, the grids were blotted in a Gatan Cryo Plunge III. The samples were quickly plunged into liquid ethane to make very thin vitrified layer. The temperature of plunging workstation was set with −175 °C. The grids were mounted on a Gatan 626 single tilt cryoholder equipped in the TEM column. The specimen and the holder tip were cooled by liquid nitrogen, which is maintained during transfer into the microscope and subsequent imaging. The imaging was performed with a JEOL 2100 FEG microscope operated at 200 kV and a magnification in the range of 10 000×−60 000×. All images were recorded on a Gatan 2000 × 2000 UltraScan CCD camera.

Photoluminescent IR Spectroscopy, UV−vis Absorption Spectroscopy, and Absolute Quantum Yield Measurements. The PL spectra of the samples were recorded at room temperature with a λ = 850 nm long-pass filter by using different kinds of IR detectors. The excitation sources for PL were λ = 532 nm at different laser power intensities (0.1 ÷ 0.8 mW) and λ = 630 nm diode lasers (Thorlabs). Most of the measurements were detected by Princeton Instruments Spectra Pro 300i spectrometer coupled to a liquid nitrogen-cooled Princeton Instruments OMA V InGaAs CCD array detector. At least three different points for samples were recorded. Some experiments were carried out either with InGaAs detector DET10N (500−1700 nm, Thorlabs) or by a NIR-Quest spectrometer from Ocean Optics. The shown absorption spectra were recorded on an 8453 UV−vis spectrometer (Agilent) or on a Cary 5000 spectrophotometer (Variant). The QY of PbS samples, in chloroform and in water, were taken using a Labsphere integrating sphere by using a 5 mW, 405 nm light as the source, chopping the beam at 210 Hz, and collecting the output using a calibrated InGaAs detector through a Stanford Research Systems lock-in amplifying system. A filter was used to spectrally separate the fluorescence, and the final quantum yield was corrected for reflectance and leakage of the filter.

■ ASSOCIATED CONTENT

Supporting Information

The Supporting Information is available free of charge on the ACS Publications website at DOI: 10.1021/acs.nanolett.7b03735.

Additional details about water-soluble QD characterization, the LHNs + QDs system (either in liquid or in solid systems), GFC particle size distribution, agarose gel electrophoresis, optical properties, cryo-TEM analysis, PL and absorption spectra, excitation measurement, and NMR spectra (PDF)

■ AUTHOR INFORMATION

Corresponding Author

*E-mail: mgb@mit.edu. Phone: 617-253-9796.

ORCID

Francesca S. Freyria: 0000-0002-2710-5545
José M. Cordero: 0000-0002-1694-4722
Justin R. Caram: 0000-0001-5126-3829
Sandra Doria: 0000-0002-9440-1643
Yue Chen: 0000-0002-9579-5189
Adam P. Willard: 0000-0002-0934-4737
Moungi G. Bawendi: 0000-0003-2220-4365

Present Address

§Department of Chemistry and Biochemistry, University of California Los Angeles, Los Angeles, CA, 900049 United States

Notes

The authors declare no competing financial interest.

■ ACKNOWLEDGMENTS

This work has been supported by Eni SpA under the Eni-MIT Alliance Solar Frontiers Center. F.S.F. gratefully acknowledges support from an MITei-ENI Fellowship. J.R.C. and A.P.W. (theoretical modeling) were funded by the Center for Excitonics, an Energy Frontier Research Center funded by the U.S. Department of Energy, Office of Science, Office of Basic Energy Sciences under award no. DE-SC0001088 (MIT). A.D. was supported by the Natural Science and Engineering Research Council of Canada Postgraduate Scholarship Doctoral (NSERC PGS D) program. Y.C. (ligand characterization) was supported by the U.S. Department of Energy, Office of Science, Office of Basic Energy Sciences, Division of Materials Science and Engineering under award no. DE-FG02-07ER46454. The authors thank Jess A. Carr for helping with surface charge imaging. The authors also thank Igor Coropceanu for discussions regarding the project.

■ REFERENCES

(1) Zhang, Q.; Atay, T.; Tischler, J. R.; Bradley, M. S.; Bulović, V.; Nurmikko, A. V. *Nat. Nanotechnol.* **2007**, *2*, 555−559.
(2) Qiao, Y.; Polzer, F.; Kirmse, H.; Steeg, E.; Kirstein, S.; Rabe, J. P. *J. Mater. Chem. C* **2014**, *2*, 9141−9148.
(3) Song, Q.; Jiao, Y.; Wang, Z.; Zhang, X. *Small* **2016**, *12* (1), 24−31.
(4) Zengin, G.; Johansson, G.; Johansson, P.; Antosiewicz, T. J.; Käll, M.; Shegai, T. *Sci. Rep.* **2013**, *3*, 1−8.
(5) Agranovich, V. M.; Gartstein, Y. N.; Litinskaya, M. *Chem. Rev.* **2011**, *111*, 5179−5214.
(6) Hildebrandt, N.; Spillmann, C. M.; Algar, W. R.; Pons, T.; Stewart, M. H.; Oh, E.; Susumu, K.; Díaz, S. A.; Delehanty, J. B.; Medintz, I. L. *Chem. Rev.* **2017**, *117*, 536−711.
(7) Halpert, J. E.; Tischler, J. R.; Nair, G.; Walker, B. J.; Liu, W.; Bulović, V.; Bawendi, M. G. *J. Phys. Chem. C* **2009**, *113*, 9986−9992.
(8) Walker, B. J.; Nair, G. P.; Marshall, L. F.; Bulović, V.; Bawendi, M. G. *J. Am. Chem. Soc.* **2009**, *131*, 9624−9625.
(9) Kirstein, S.; Daehne, S. *Int. J. Photoenergy* **2006**, *2006*, 1−21.
(10) Eisele, D. M.; Knoester, J.; Kirstein, S.; Rabe, J. P.; Vanden Bout, D. A. *Nat. Nanotechnol.* **2009**, *4*, 658−663.
(11) Hestand, N. J.; Spano, F. C. *Acc. Chem. Res.* **2017**, *50*, 341−350.
(12) von Berlepsch, H.; Kirstein, S.; Böttcher, C. *J. Phys. Chem. B* **2004**, *108*, 18725−18733.
(13) Eisele, D. M.; Cone, C. W.; Bloemsma, E. A.; Vlaming, S. M.; van der Kwaak, C. G. F.; Silbey, R. J.; Bawendi, M. G.; Knoester, J.; Rabe, J. P.; Vanden Bout, D. A. *Nat. Chem.* **2012**, *4*, 655−662.
(14) von Berlepsch, H.; Kirstein, S.; Hania, R.; Pugžlys, A.; Böttcher, C. *J. Phys. Chem. B* **2007**, *111*, 1701−1711.
(15) Eisele, D. M.; Arias, D. H.; Fu, X.; Bloemsma, E. A.; Steiner, C. P.; Jensen, R. A.; Rebentrost, P.; Eisele, H.; Tokmakoff, A.; Lloyd, S.; Nelson, K. A.; Nicastro, D.; Knoester, J.; Bawendi, M. G. *Proc. Natl. Acad. Sci. U. S. A.* **2014**, *111*, E3367−E3375.
(16) Clark, K. A.; Krueger, E. L.; Vanden Bout, D. A. *J. Phys. Chem. C* **2014**, *118*, 24325−24334.
(17) Chuang, C.-H. M.; Brown, P. R.; Bulović, V.; Bawendi, M. G. *Nat. Mater.* **2014**, *13*, 796−801.

DOI: 10.1021/acs.nanolett.7b03735
Nano Lett. 2017, 17, 7665−7674

(18) Carey, G. H.; Abdelhady, A. L.; Ning, Z.; Thon, S. M.; Bakr, O. M.; Sargent, E. H. *Chem. Rev.* **2015**, *115*, 12732−12763.
(19) Akselrod, G. M.; Weidman, M. C.; Li, Y.; Argyropoulos, C.; Tisdale, W. A.; Mikkelsen, M. H. *ACS Photonics* **2016**, *3*, 1741−1746.
(20) Moreels, I.; Lambert, K.; Smeets, D.; De Muynck, D.; Nollet, T.; Martins, J. C.; Vanhaecke, F.; Vantomme, A.; Delerue, C.; Allan, G.; Hens, Z. *ACS Nano* **2009**, *3*, 3023−3030.
(21) Geyer, S. M.; Scherer, J. M.; Jaworski, F. B.; Bawendi, M. G. *Opt. Mater. Express* **2013**, *3*, 1167−1175.
(22) Murray, C. B.; Nirmal, M.; Norris, D. J.; Bawendi, M. G.Z. *Z. Phys. D: At., Mol. Clusters* **1993**, *26*, 231−233.
(23) Hines, M. A.; Scholes, G. D. *Adv. Mater.* **2003**, *15* (21), 1844−1849.
(24) Weidman, M. C.; Beck, M. E.; Hoffman, R. S.; Prins, F.; Tisdale, W. A. *ACS Nano* **2014**, *8*, 6363−6371.
(25) Cademartiri, L.; Bertolotti, J.; Sapienza, R.; Wiersma, D. S.; von Freymann, G.; Ozin, G. A. *J. Phys. Chem. B* **2006**, *110*, 671−673.
(26) Jing, L.; Kershaw, S. V.; Li, Y.; Huang, X.; Li, Y.; Rogach, A. L.; Gao, M. *Chem. Rev.* **2016**, *116*, 10623−10730.
(27) Deng, D.; Xia, J.; Cao, J.; Qu, L.; Tian, J.; Qian, Z.; Gu, Y.; Gu, Z. *J. Colloid Interface Sci.* **2012**, *367*, 234−240.
(28) Hyun, B.-R.; Chen; Rey, D. A.; Wise, F. W.; Batt, C. A. *J. Phys. Chem. B* **2007**, *111*, 5726−5730.
(29) Zhao, H.; Wang, D.; Chaker, M.; Ma, D. *J. Phys. Chem. C* **2011**, *115*, 1620−1626.
(30) Zhang, Y.; Schnoes, A. M.; Clapp, A. R. *ACS Appl. Mater. Interfaces* **2010**, *2*, 3384−3395.
(31) Kalsin, A. M.; Kowalczyk, B.; Wesson, P.; Paszewski, M.; Grzybowski, B. A. *J. Am. Chem. Soc.* **2007**, *129*, 6664−6665.
(32) Jumabekov, A. N.; Deschler, F.; Böhm, D.; Peter, L. M.; Feldmann, J.; Bein, T. *J. Phys. Chem. C* **2014**, *118*, 5142−5149.
(33) Wang, C.; Kodaimati, M. S.; Schatz, G. C.; Weiss, E. A. *Chem. Commun.* **2017**, *53*, 1981−1984.
(34) Wang, C.; Weiss, E. A. *J. Am. Chem. Soc.* **2016**, *138*, 9557−9564.
(35) Dubertret, B.; Skourides, P.; Norris, D. J.; Noireaux, V.; Brivanlou, A. H.; Libchaber, A. *Science* **2002**, *298*, 1759−1762.
(36) Bruchez, M., Jr.; Moronne, M.; Gin, P.; Weiss, S.; Alivisatos, A. P. *Science* **1998**, *281*, 2013−2016.
(37) Nakane, Y.; Tsukasaki, Y.; Sakata, T.; Yasuda, H.; Jin, T. *Chem. Commun.* **2013**, *49*, 7584−7586.
(38) Chen, J.; Kong, Y.; Wang, W.; Fang, H.; Wo, Y.; Zhou, D.; Wu, Z.; Li, Y.; Chen, S. *Chem. Commun.* **2016**, *52*, 4025−4028.
(39) Levina, L.; Sukhovatkin, V.; Musikhin, S.; Cauchi, S.; Nisman, R.; Bazett-Jones, D. P.; Sargent, E. H. *Adv. Mater.* **2005**, *17*, 1854−1857.
(40) Ma, N.; Marshall, A. F.; Rao, J. *J. Am. Chem. Soc.* **2010**, *132*, 6884−6885.
(41) Clapp, A. R.; Medintz, I. L.; Fisher, B. R.; Anderson, G. P.; Mattoussi, H. *J. Am. Chem. Soc.* **2005**, *127*, 1242−1250.
(42) Caram, J. R.; Doria, S.; Eisele, D. M.; Freyria, F. S.; Sinclair, T. S.; Rebentrost, P.; Lloyd, S.; Bawendi, M. G. *Nano Lett.* **2016**, *16*, 6808−6815.
(43) Basko, D.; La Rocca, G. C.; Bassani, F.; Agranovich, V. M. *Eur. Phys. J. B* **1999**, *8*, 353−362.
(44) Agranovich, V. M.; Basko, D. M. *JETP Lett.* **1999**, *69*, 250−254.
(45) Plehn, T.; Ziemann, D.; Megow, J.; May, V. *J. Phys. Chem. B* **2015**, *119*, 7467−7472.
(46) Qiao, Y.; Polzer, F.; Kirmse, H.; Steeg, E.; Kühn, S.; Friede, S.; Kirstein, S.; Rabe, J. P. *ACS Nano* **2015**, *9*, 1552−1560.
(47) Wang, C.; Weiss, E. A. *Nano Lett.* **2017**, *17*, 5666−5671.
(48) McHale, J. L. *J. Phys. Chem. Lett.* **2012**, *3*, 587−597.
(49) Tummeltshammer, C.; Portnoi, M.; Mitchell, S. A.; Lee, A.; Kenyon, J.; Tabor, A. B.; Papakonstantinou, I. *Nano Energy* **2017**, *32*, 263−270.
(50) Anikeeva, P. O.; Madigan, C. F.; Halpert, J. E.; Bawendi, M. G.; Bulović, V. *Phys. Rev. B: Condens. Matter Mater. Phys.* **2008**, *78*, 85434.
(51) Wang, C.; Thompson, R. L.; Ohodnicki, P.; Baltrus, J.; Matranga, C. *J. Mater. Chem.* **2011**, *21*, 13452.
(52) Tsurumi, T.; Hirayama, H.; Vacha, M.; Taniyama, T. *Nanoscale physics for materials science*; Taylor & Francis Group: Abingdon, UK; 2010; pp 133−140.
(53) He, X.; Ma, N. *Colloids Surf., B* **2014**, *124*, 118−131.
(54) Hildebrandt, N. *FRET - Förster Resonance Energy Transfer: From Theory to Applications* **2014**, 105−163.
(55) Clark, K. A.; Cone, C. W.; Vanden Bout, D. A. *J. Phys. Chem. C* **2013**, *117*, 26473−26481.

DOI: 10.1021/acs.nanolett.7b03735
Nano Lett. 2017, 17, 7665−7674